tion with a difference between extremes of about 0.2 mbar. The minimum occurs about 4 hours after noon and the maximum at about 4 hours after midnight. Figures 1 to 4 exhibit this diurnal behavior even though the digitization increment of the data is a substantial fraction of the amplitude detected. The mean pressure for sols 1 to 3 is 7.65 mbar. It is worthy of note that an amplitude of 0.1 mbar is in excess of 1 percent of the mean. On Earth, that would be a diurnal amplitude greater than 10 mbar, very much larger than what is observed (about 1.5 mbar).

Finally, we note that neither the magnitude nor the direction of the measured winds is consistent with the aeolian (wind-formed) features identified in lander images (*8*). We conclude that these features were produced during another martian season, or another epoch.

S. L. HESS
Florida State University, Tallahassee
R. M. HENRY
NASA Langley Research Center, Hampton, Virginia
C. B. LEOVY
University of Washington, Seattle
J. A. RYAN
California State University, Fullerton
J. E. TILLMAN
University of Washington, Seattle
T. E. CHAMBERLAIN
TRW, Inc., Redondo Beach, California
H. L. COLE
National Center for Atmospheric Research, Boulder, Colorado
R. G. DUTTON
Martin Marietta Aerospace, Denver, Colorado
G. C. GREENE
NASA Langley Research Center
W. E. SIMON
Martin Marietta Aerospace
J. L. MITCHELL
Florida State University

References and Notes

1. T. E. Chamberlain, H. L. Cole, R. G. Dutton, G. C. Greene, J. E. Tillman, *Bull. Am. Meteorol. Soc.*, in press.
2. All directions are measured clockwise from planetary north.
3. The approximate landing point is 22.3°N, 48.0°W.
4. The term "sol" refers to the martian day of 24.660 hours and is used to avoid confusion with the terrestrial day.
5. Topographic map of Lunae Pallas Quadrangle of Mars, MC10, M5M 15/16 RCM, 1976 (U.S. Geological Survey, Reston, Va. 22092).
6. R. W. Zurek, *J. Atmos. Sci.* **33**, 321 (1976); S. Chapman and R. S. Lindzen, *Atmospheric Tides* (Gordon & Breach, New York, 1970).
7. H. H. Kieffer, S. C. Chase, Jr., E. D. Miner, F. D. Palluconi, G. Münch, G. Neugebauer, T. Z. Martin, *Science* **193**, 780 (1976).
8. T. A. Mutch, A. B. Binder, F. O. Huck, E. C. Levinthal, S. Liebes, Jr., E. C. Morris, W. R. Patterson, J. B. Pollack, C. Sagan, G. R. Taylor, *ibid.*, p. 791.
9. Supported by NASA contract NAI 9693.

27 July 1976

The Surface of Mars: The View from the Viking 1 Lander

Abstract. *The first photographs ever returned from the surface of Mars were obtained by two facsimile cameras aboard the Viking 1 lander, including black-and-white and color, 0.12° and 0.04° resolution, and monoscopic and stereoscopic images. The surface, on the western slopes of Chryse Planitia, is a boulder-strewn deeply reddish desert, with distant eminences—some of which may be the rims of impact craters—surmounted by a pink sky. Both impact and aeolian processes are evident. After dissipation of a small dust cloud stirred by the landing maneuvers, no subsequent signs of movement were detected on the landscape, and nothing has been observed that is indicative of macroscopic biology at this time and place.*

On 20 July 1976, at 1613 after local Mars midnight, the Viking 1 spacecraft touched down on the surface of Mars and immediately began transmission of photographs to Earth. Camera 2 on the Viking 1 lander obtained the first photographs ever returned from the surface of Mars—a high-resolution view of the vicinity of Viking lander footpad 3 in the near field (Fig. 1) and a low-resolution panoramic view of the middle to far field, including the sky of Mars (Fig. 2).

The Viking lander camera (*1, 2*) is basically a multispectral radiometer with an optical-mechanical scanning mechanism that determines both the image raster and the field of view. It features an array of 12 silicon photodiodes consisting of four broadband channels with selectable focus for high-resolution imaging, one broadband channel for rapid surveys, six narrowband (about 0.1 μm) channels for multispectral imaging (color and near-infrared), and one narrowband channel for scanning the sun. The instantaneous fields of view are 0.04° for the four high-resolution channels and 0.12° for the other channels. The field of view ranges in elevation from 40° above to 60° below the horizon, and in azimuth from 0° to 342.5°. The camera scanning rates are synchronized to the lander data transmission rates of 16,000 bit/sec to the two orbiters as relay stations and 250 bit/sec directly to Earth. Image data can also be secured at preferred times and stored on a lander tape recorder for later transmission to take advantage of favorable imaging periods (for example, sun elevation angles).

High sensitivity is obtained over a wide dynamic range with only 6-bit encoding by the use of six commandable linear gains and 32 offsets. This approach was expected to require some initial trials in selecting optimum dynamic ranges after landing (*3*). However, once the atmosphere and surface brightness was approximately characterized from initial image data, it was possible to select optimum dynamic ranges for subsequent imagery and radiometry experiments.

General geological setting. The Viking 1 landing site (22.47° ± 0.15°N, 48.0° ± 0.5°W, areographic coordinates) is located about 130 km to the east of Lunae Planum, on the western slopes of the large depression, Chryse Planitia (*4*). The Chryse basin is about 5 km deep and the landing site lies about 2 km higher than the floor. Lunae Planum is separated from the more sparsely cratered Chryse Planitia by an irregular, scarplike boundary. Viking orbiter imagery shows a num-

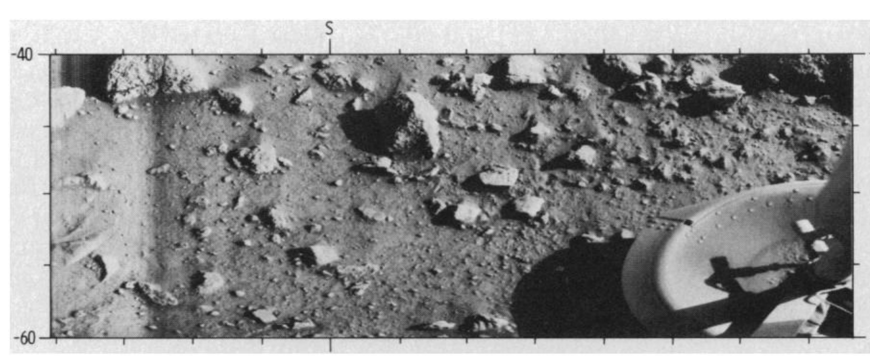

Fig. 1. This high-resolution picture of footpad number 3 and the adjacent surface is the first image ever returned from the surface of Mars. The large rock near the center is about 10 cm across. Some of the rocks have a vesicular appearance; one in the upper right has a horizontally banded texture. Some of the texture in the smooth parts of the surface was probably produced during landing; in particular a few elongate pits near the center appear to have been produced by the impact of small pebbles thrown out by the rocket exhaust. Sediment, including small pebbles or clods, has been deposited in the concave footpad. At left are angular rocks with adjacent sediment piles. At right center is a rock which seems to have been moved about its own length to the right. It is just conceivable that the retrorocket exhaust during landing produced this offset. Refer to Fig. 3 for an orthographic sketch map of this terrain.

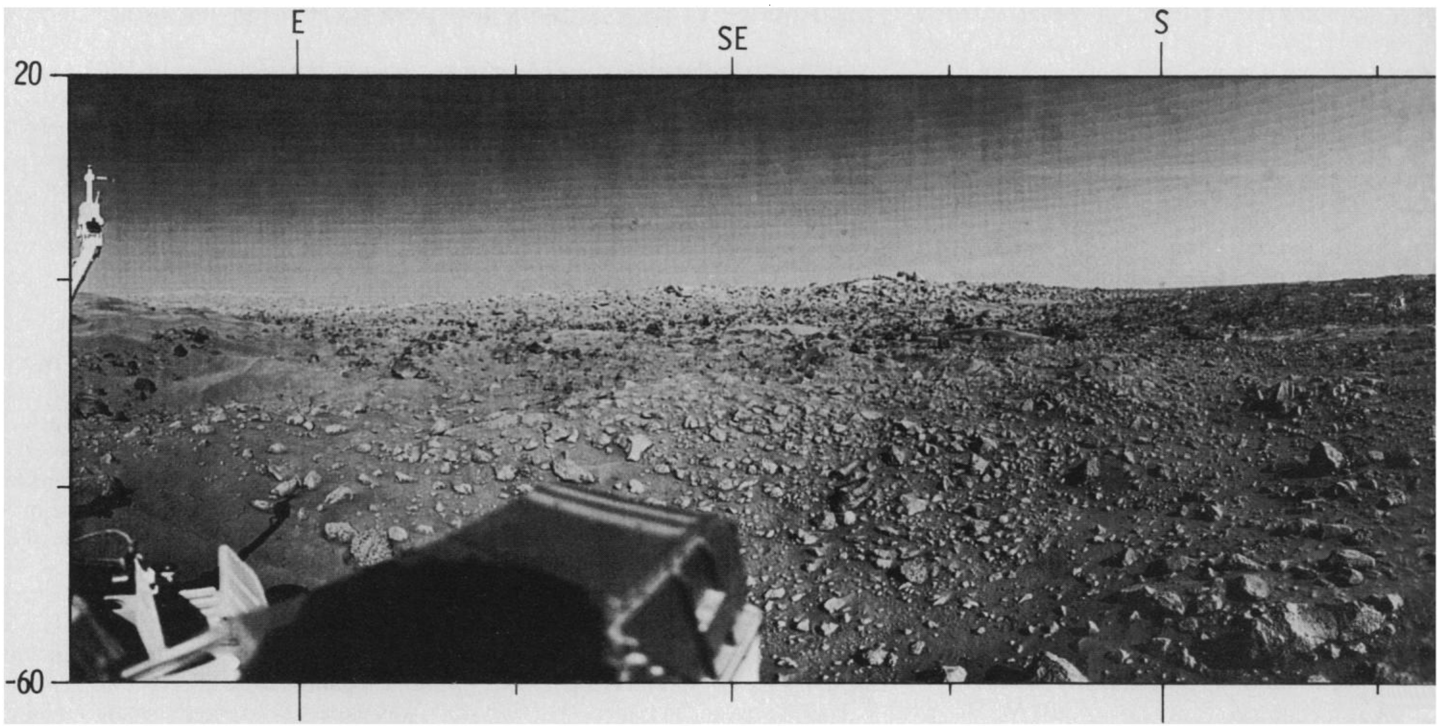

Fig. 2. This low-resolution panorama of the martian landscape was taken on sol 0 by camera 2. The left side, where part of the surface sampler is visible, is looking east-northeast on Mars. The other edge is northwest. The sky is brighter in the direction of the setting sun. Some of the irregularities on the skyline, particularly the one to the southeast, may be parts of the raised rims of impact craters. A shallow depression occurs in the foreground just to the right of center, and may be a shallow 3-m-diameter impact crater, possibly a secondary. At this resolution an object 6 m in size subtends one picture element at the nominal horizon. The apparent horizon sinusoid is an artifact of camera tilt (see also Fig. 5).

ber of large, scoured channels that emerge from the edge of Lunae Planum and trend eastward toward the landing site. However, no specific evidence for channeling can be seen at the landing site itself. Rather, the site can be characterized as topographically smooth at the scale of the orbiter photographs. The principal contributions to topographic relief are craters and ridges similar to those on the lunar maria. Some of the ridges west of the landing site appear to postdate the fluvial features; in other cases they are clearly cut by the channels. The regional plains unit is sparsely cratered and may be interpreted as composed largely of volcanic deposits: lunarlike ridges and uniformly flooded craters are both in evidence.

On the basis of regional relations, several models for the recent history of the site are possible: (i) the Chryse plains are predominantly volcanic, but the fluvial channels to the west have emplaced a smooth deposit in the landing area; (ii) the Chryse plains are volcanic and in part are younger than the channel deposits, particularly in the landing area; or (iii) the channel deposits are younger than the plains, but do not reach the landing site area. Among the processes inferred to have operated at the landing site are fluvial activity, flood volcanism, ridge formation, impact cratering, aeolian abrasion and transport, and chemical weathering. The last three of these processes have operated most recently. Orbiter pictures indicate that impact cratering has modified the area since the emplacement of the plains surface. The general indication from crater densities on various surfaces is that volcanism and fluvial modification of the region were not separated greatly in time (*4*).

Description of the surface of Mars. We first describe the initial images returned by the Viking lander cameras. The first high-resolution picture of Mars (Fig. 1) covers some 57.5° in azimuth in the near field. A circular arc concentric with the camera and of radius 1.9 m would pass through the center of the image. A map of objects in this near-field photograph is displayed in Fig. 3. The large fractured rock in the upper left of Fig. 1 is about 20 cm across. Both blocky and angular rocks are apparent, as well as finer-grained lower-albedo matrix material between the rocks reminiscent of a desert armor or pavement in which the fine-grained particles have been transported by aeolian processes, leaving behind coarser material similar to a gravel. Many of the rocks are fairly angular. Such rocks indicate (i) that the rock was recently produced or fractured; (ii) that the rock, if ancient, was long buried and shielded from erosional processes and only recently exhumed to view; or (iii) that the rock is old but that aeolian or other erosional processes in this region of Mars are feeble.

Several larger rocks exhibit irregular and pitted surfaces, and the large rock in the upper left of Fig. 1 displays intersecting linear cracks. Extending downward from this rock toward the camera is a linear vertical dark band, which may be due to a partial obscuration of the martian landscape for some tens of seconds due to clouds or dust intervening between the sun and the surface (*5*). Associated with several of the rocks are apparent signs of wind transport of granular material. Sand and dust were deposited during landing inside the footpad near its contact with the support strut. Small streaks and small pits near the footpad were probably caused by the landing event, the footpad kicking out material on contact with the surface.

Much detail is clearly evident in shadows; the illumination of shadows may be due both to the significant light scattering by dust in the martian atmosphere and to reflection off the surface of the spacecraft itself. The sun is to the right and shadows are cast to the left.

In the Viking 1 sol 0 panorama (Fig. 2) a view of about 300° was photographed in a single image. It consists of 2500 lines, each comprising 512 picture ele-

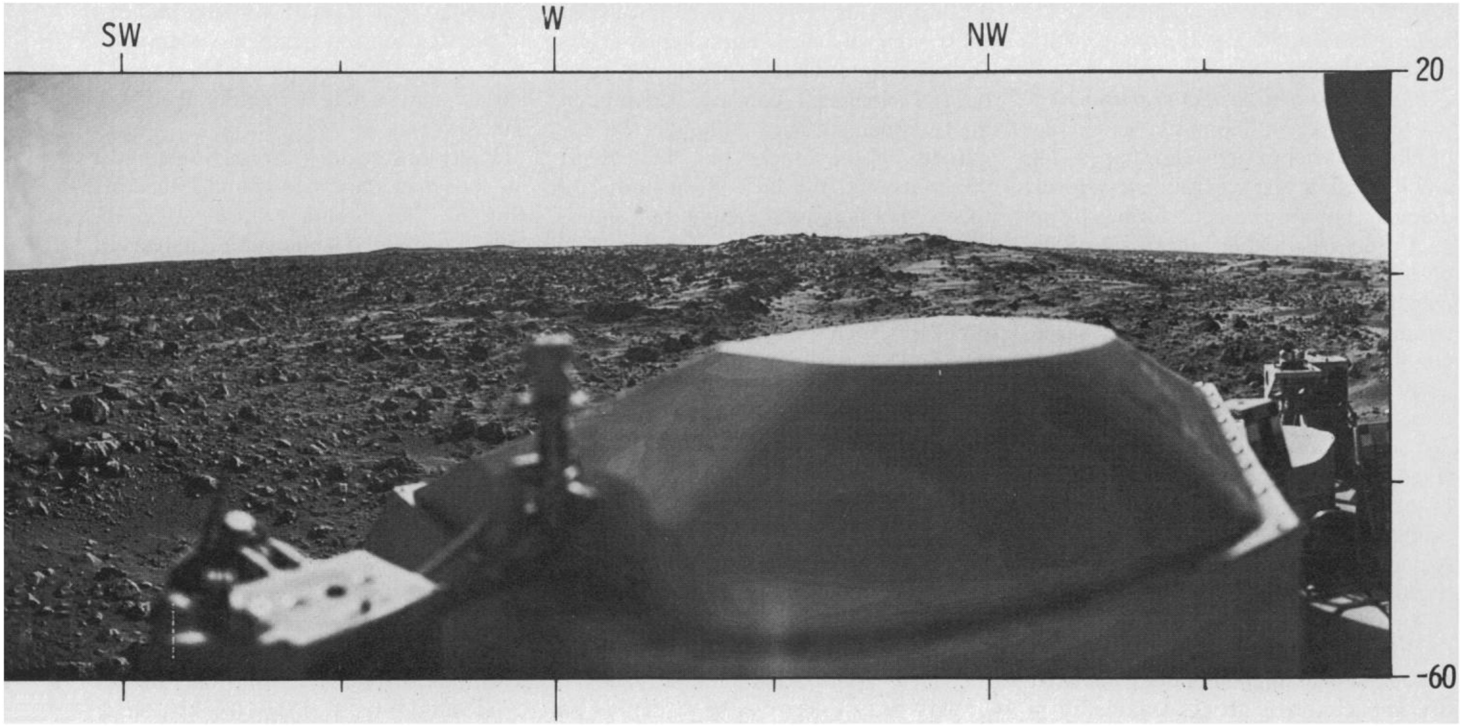

ments. Each picture element subtends 0.12° at the camera in this survey mode. The panorama is here described in sequence from left to right.

The deployed Viking meteorology boom, seen toward the east-northeast, was caged before deployment in the white cradle seen directly below. The out-of-focus spacecraft component seen in the southeast foreground of the panorama is the housing for the Viking sample arm, which is not deployed at this time. The arm and its housing are pivoted toward the spacecraft. On the ground can be seen the shadow of the meteorology boom.

The parallel lines in the sky are an artifact of the intensity digitization of the Viking lander camera and are not real features. However, the change of brightness from horizon toward zenith (and from east to southwest) is accurately reflected in this picture, obtained in late martian afternoon. At the eastern horizon to the left is a plateaulike prominence much brighter than the foreground material, perhaps because it is illuminated directly by the low sun. The plateau may be the rim of a large impact crater.

The topography of the landing site is gently rolling (as is dramatically revealed by fusing the stereo pair on the cover). In the foreground, interblock regions are darker than blocks; in the background, in contrast, blocks are darker than interblock regions. The martian nominal horizon is approximately 3 km away; however, nearby hills obscure our view of large segments of the far horizon, and distant eminences may project above the nominal horizon.

At the left of the panorama is a field of apparent small sand dunes, across which extends a band of dark boulders which continues across the panorama to the southwestern horizon. Subparallel, sinuous ridges are superimposed on the fine-grained patch in the eastern foreground.

The dark knob on the southern horizon may be composed of one or more large boulders. The dark, relatively rock-free foreground region to the southwest is a shallow, circular depression. This depression and others like it may be secondary craters. A horizontal cloud stratum can be made out about halfway between the horizon and the top of Fig. 2 in a southerly direction.

In the west foreground is the low-gain S-band antenna for receipt of commands from Earth. It is in front of the radioisotope thermoelectric generator (RTG-2), which provides the spacecraft with its electrical power. Several projections on or near the horizon may represent the remains of distant impact craters.

A continuation of the right foreground of the panorama (Fig. 4) reveals the color chart for lander camera calibration, the mirror for the Viking magnetic properties experiment, the microdot [see (*22*)], and parts of a 10 by 10 inch grid on the upper surface of the lander, as well as the high-gain S-band antenna now properly deployed for direct communication between the spacecraft and Earth. A rock can be made out just to the left of the S-band antenna support, which appears to be undercut on one side and partially buried by drifting grains on the other. In the right background are patches of smooth fine-grained material which define the beginning of a large dune field off to the right of the picture; its continuation is seen in the sol 3 panorama (Fig. 5).

The survey taken on sol 3 (Fig. 5) completes coverage of the approximately 60° of azimuth not covered on the sol 0 panorama (Fig. 2). A map of objects in this panorama is shown as Fig. 6. In the northeast is seen the upper part of the strut of footpad 2 and the deployed meteorology boom which extends through the right center of the image. Continuing from the vicinity of the spacecraft toward the horizon behind the meteorology boom is an irregular field of fine-grained material in the form of large ripples and dunes. Both dark and bright rocks extend into this part of the scene. The bright rocks form a small rocky hill just above the RTG housing in the image center and continue across the foreground. Several of these rocks, particularly those in the right foreground, are adjacent to depressions apparently scoured by the wind. Dark rocks are abundant to image right farther from the spacecraft and are partly covered by the dunes. An especially prominent dark rock in the northeast (about 8 m away) is about 3 m wide and 1 m high. Several other large dark boulders are seen toward the horizon. In general, the far horizon appears as a bright band. Horizon detail is particularly prominent to the right, where an accumulation of large boulders and possible outcrops can be seen (see Fig. 7).

Blocks and their size distribution. The images display an impressive abundance of blocks of many sizes and shapes. The blocks near the spacecraft are coarsely granular, possibly breccias formed by impact processes. Other blocks are pitted, possibly reflecting a vesicular texture. One block has an indication of rough striations, suggestive of layered basalt. On the horizon, which is about 3 km away for a spherical surface, at least three topographically high regions reminiscent of crater profiles can be seen (Figs. 2 and 5). The change is brightness of the surface from dark near the sun to bright at 180° away in azimuth is primarily due to illumination: features are backlit close to the sun and frontlit 180° away.

Any azimuth alignment of long axis directions of blocks remains to be determined. If such alignment does not exist, the implication is that streamlining by fluid (water or wind) has not occurred, or has since been altered. That interpretation is consonant with the angularity of most of the blocks. Several rocks in the field of view do, however, exhibit unusual shapes. South of southeast (Figs. 2 and 5) are two peculiarly shaped rocks, one of which has a tapering cylindrical cross section, while the other has an elongated concave indentation in its upper surface. Although the angularity of the blocks may be due to wind-faceting, the lack of clustering of facets in particular azimuths argues against this hypothesis.

Rocks of unusual forms can be produced by various physical weathering processes such as frost shattering, spalling, and aeolian sandblasting. Some of these unusual forms resemble technological artifacts or biological forms (*6*). Care must be exercised in interpreting the rocks seen in the Viking pictures. Some rocks in these pictures appear to have unusual shapes and surface markings, which are, however, due to highlights and shadows cast by irregularities on the rock surface. The true shapes of rocks can be determined only by viewing them at a variety of illumination angles.

Very few craters can be discerned on the panoramas (Figs. 1 and 5). Our first estimate is that crater area densities on the martian surface are several orders of magnitude below impact saturation for crater sizes less than about 50 m. However, there may be a number of shallow secondary craters that would be difficult to detect from our perspective. In addition, some of the smooth patches on the survey images may be craters filled with sand or dust.

Interblock regions are covered by or composed of smooth to granular surfaces (Fig. 8). The smooth surfaces are probably fine-grained sediments. Analysis of the high-resolution imagery indicates that the fines are < several hundred micrometers in size.

Block size distributions were tabulated using the sol 0 survey image for a region from southeast to southwest and from − 15° to − 40° in elevation (see Fig. 3). Those coordinates translate to a 15.48-m^2 area on Mars with a poorest resolution of 1 cm and a best resolution of 0.4 cm. Counts were truncated below three times the poorest resolution. The resulting size distribution, normalized to 100 m^2, is shown in Fig. 9, along with counts from Surveyor 3 and Surveyor 7 locations on the moon (*7*). The block size distribution is similar to that obtained with Surveyor 7, which landed within one crater radius of Tycho, a crater 85 km in diameter. The Surveyor 7 location is unique in lunar landings, exhibiting a surface with a thin regolith and

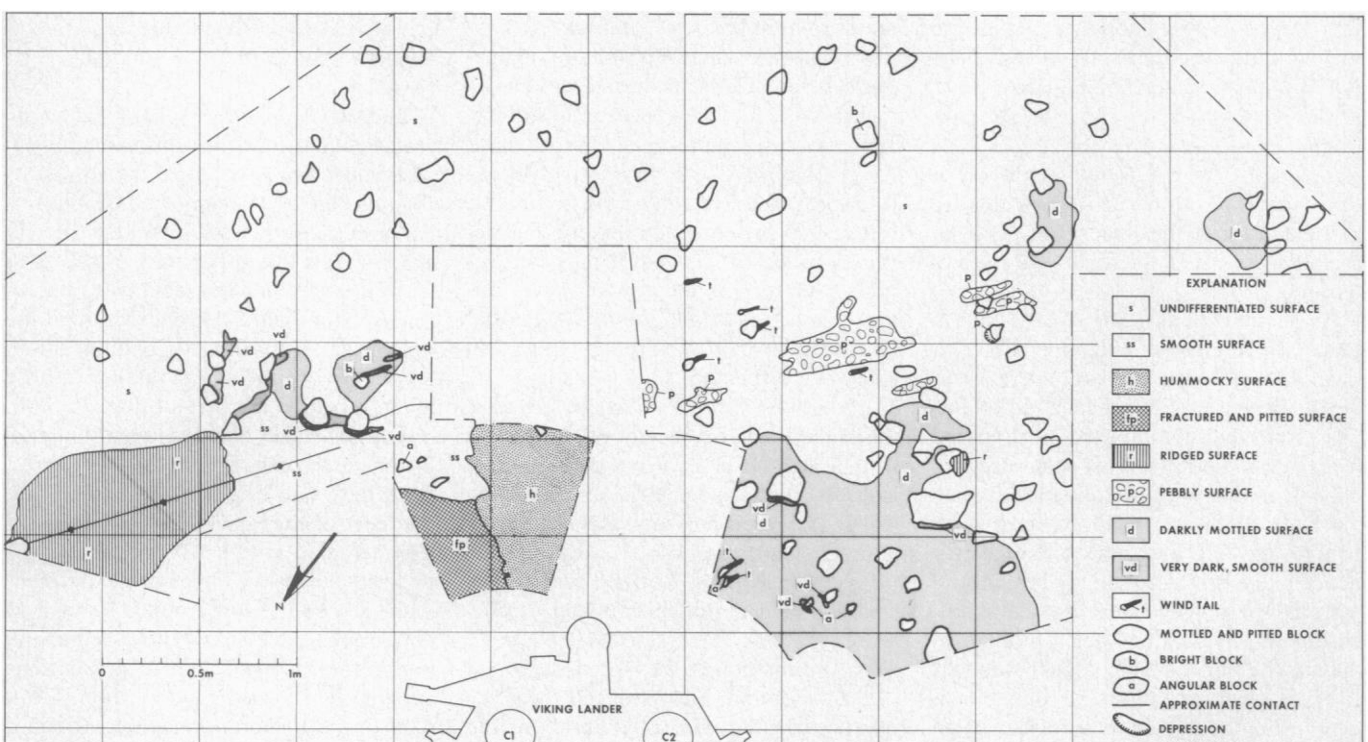

Fig. 3. Orthographic sketch map of terrain immediately surrounding the Viking 1 lander. The following units are found: mottled and pitted blocks (heavy lines); (*a*) angular blocks with smooth, flat sides; (*b*) bright, smooth, rounded blocks; (*d*) mottled surface having smooth, dark patches of fine-grained material; (*h*) hummocky surface composed of small clods emplaced during landing; (*fp*) fractured, pitted, and grooved surface resulting from disturbances during landing; (*p*) pebbly surface having a less reddish hue than the undifferentiated surface, and interpreted to be an aeolian lag gravel; (*r*) fine sinuous ridges on smooth surface; (*s*) undifferentiated surface having small blocks interspersed with fine-grained material of generally reddish hue; (*ss*) smooth surface with few blocks; (*t*) tapering reddish deposits on the lee side of boulders, interpreted to be wind tails; (*vd*) very dark surface composed of fine-grained smooth material that is deposited mostly in depressions, and against and on top of some boulders; and horseshoe-shaped depressions interpreted to be scour marks on the windward side of blunt blocks (shown in Fig. 10).

abundant blocks. Tycho is only 100 million years old (*8*) and, within a crater radius, postcratering events have served only to excavate blocky ejecta, with minimum generation of fine-grained regolith. With more data on larger block sizes, the size distribution curve would allow (*9*) estimates to be made on the landing hazard due to blocks.

At least three possible impact craters can be seen in the sol 0 survey image, providing positive evidence for one process capable of producing a regolith. The angularity of the block also argues for production by fracturing, most likely by mechanical crushing. The possible bedrock outcrops on the sol 0 survey images between $-4°$ and $-7°$ elevation south of southwest together with the fact that boulders seem to become larger close to the rim of the possible crater south of southeast argues for production of regolith by impact into coherent strata. But a range of other processes may also be operating, as already mentioned.

Fig. 4. This is a part of the sol 0 panorama, directly adjacent to (and to the right of) the region shown in Fig. 2. The boulder seen just above the reference test chart has a patch of dune material piled on its left side. One of three reference test targets used to calibrate the cameras is in the center of the image. Just to right of the test target is a plaque with the microdot signatures of the 10,000 participants in the Viking program.

Evidence for aeolian activity. To the south of the spacecraft, several features commonly found on desert floors can be seen. Small, flat patches of pebbly ground lie at a lower level than adjacent fine-grained materials (Fig. 8). This pebbly surface has the appearance of a lag gravel, indicating scouring by wind and removal of fine-grained material. Crescentic depressions occur adjacent to some boulders. Opposite the scour marks, some boulders exhibit fine-grained deposits with thin ridge crests. The consistent direction of these deposits and the presence of scour marks suggest that both are caused by the wind action, scours being on the windward, tails on the leeward sides of the boulders. Such features resemble wind tails commonly observed in terrestrial deserts, where sand accumulates in the aerodynamically quiescent zone immediately downwind of obstacles. Very prominent scour marks on boulders can be seen to the east of the spacecraft (Fig. 10).

The indicated wind direction derived from measurements of the directions of 43 tails of fine-grained material in these images is $197° \pm 14°$ clockwise from the north. A similar wind direction can be inferred from the accumulation of fine-grained material adjacent to the large boulder visible just below the high-gain antenna, if the material has accumulated downwind (Fig. 4). In a larger scale of kilometers to tens of kilometers, Mariner 9 (*10*) and Viking orbiter (*4*) imagery reveal both bright and dark streaks in the lees of craters and other obstacles. The flow direction indicated by Mariner 9 bright streaks is about 225° clockwise from north, suggesting that dominant sediment transport occurs during major dust storms. Mariner 9 bright streaks are most likely produced by high winds acting on deposits of fine-grained material recently settled out of the atmosphere during the last stages of the 1971–1972 global dust storm (*10*).

An extended field of apparently fine-grained material is also visible to the east of Viking 1. Brightness variations within this field suggest transverse dune crests. The lower left-hand corner of the survey image contains curvilinear dark lines that may be ripple crests.

The areas containing abundant wind tails and fine-grained deposits are bright and relatively redder on the color images. The pebbly areas of lag are slightly less red. A third material is considerably grayer in color and lower in albedo. It is very fine-grained and smooth in appearance, and occurs both banked against the bases of some boulders and astride the tops of others (Fig. 3). It also thinly covers the ground in this area, and causes the surface to look slightly mottled. This dark material may be superposed on red sand although the contrary possibility is not ruled out. It could be material moved by winds at the saltation threshold, or deposited from a cloud of dust raised during landing. It may be significant that this dark material does not have the red color that is present on the other fine-grained material associated with the wind tails.

Surface coloration. The striking reddish coloration of the martian surface, revealed by Viking lander photography (cover), has of course been anticipated by telescopic and naked-eye observations extending to prehistoric times. But we now see that the coloration applies to boulders, rocks, and fine grains; indeed it is a rare patch of the accessible surface which is not vividly reddened. The observed color hues and saturations are, we believe, accurately rendered (*11*); from terrestrial experience they are strongly reminiscent of limonite.

Limonite is a poorly defined mixture of minerals, comprised chiefly of goethite and hematite and often written as $FeO \cdot OH \cdot nH_2O$. It has been proposed before for Mars on a variety of photometric and polarimetric grounds (*12*). However, it seems clear from analysis of the Mariner 9 infrared spectrometric observations of dust suspended in the martian atmosphere that this dust, at least, cannot be composed primarily of limonite (*13*). It is a natural suggestion that the limonite is present as a relatively thin coating of "desert varnish," as first proposed by Binder and Cruikshank and Van Tassel and Salisbury (*12*). The uniformity of this coating on the martian surface suggests that the coloring mechanism is efficient and is operating in geologically recent epochs.

The limonite stain observed on the fines and rocks of terrestrial deserts is produced by the oxidation and hydration of the mafic minerals of the rocks themselves, and in most cases these rocks are igneous. If the limonite observed on the martian rocks and fines were produced in the same way, then the stain must be a fossil from an earlier period in martian history when the atmosphere was richer in H_2O and O_2 than it is today: limonite cannot be formed by the usual weathering processes under the current martian atmospheric conditions. However, there is considerable evidence to suggest that at least liquid water was abundant on the surface in the past and so the possibility that the limonite surface stain is a fossil is not without support. Alternatively (*14*), the limonite could have been produced by photooxidation of the mafic minerals in the rocks in the presence of the small amounts of water currently available in the martian surface environment. This process occurs on Mars and not on Earth because of the high martian surface flux of solar ultraviolet radiation. At the present, neither of these two modes of origin for limonite can be excluded and it seems possible that both have played a role in producing the rusty color of the martian surface on images by Viking 1.

Atmospheric properties. Images obtained by the Viking lander cameras offer a unique opportunity to study separately the surface and sky of Mars. Except for studies of the planetary limb, Mars light observed from above its atmosphere typically contains contributions from both the sky and the surface.

All quantitative estimates of sky and surface brightness are based on ground-based calibration of the cameras before launch (*2*). Little change in camera response has been observed since launch on the basis of periodic use of the inter-

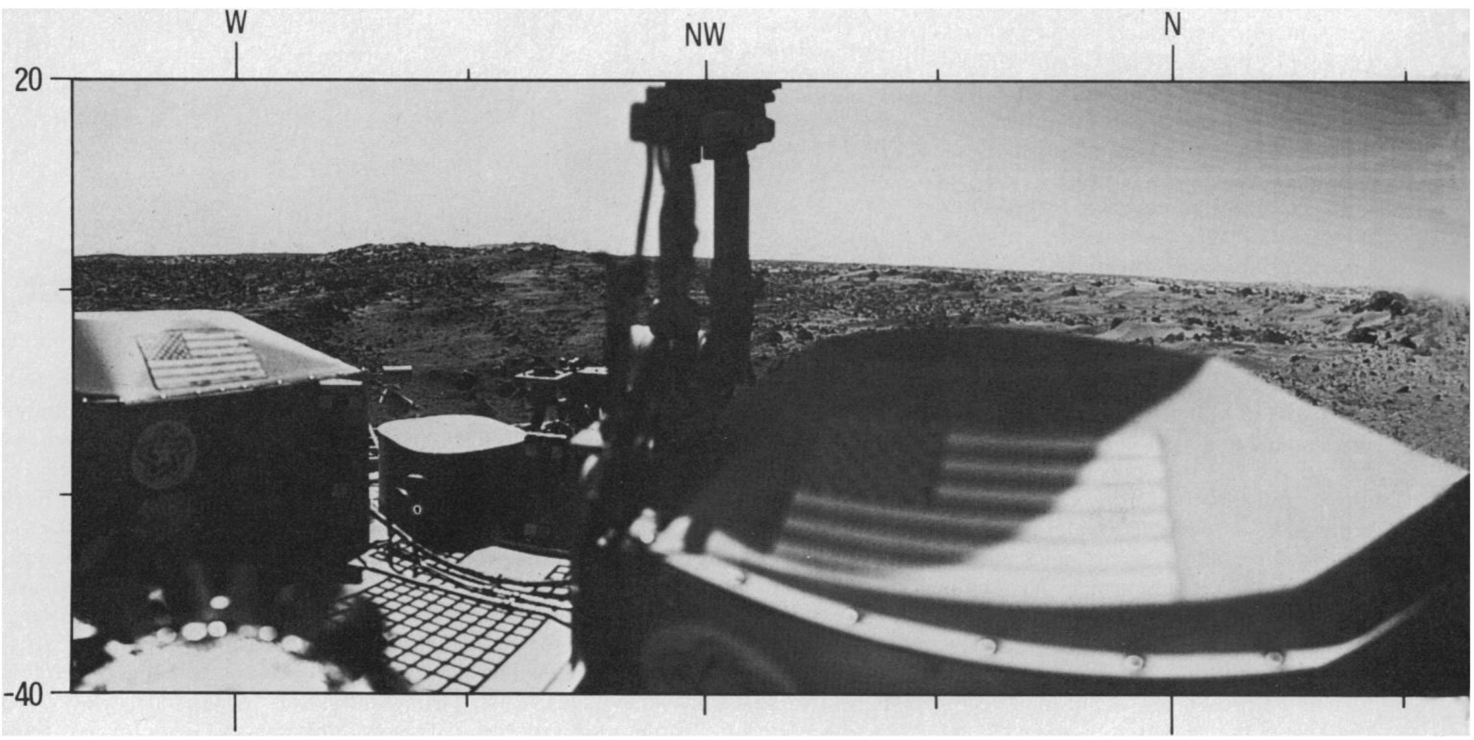

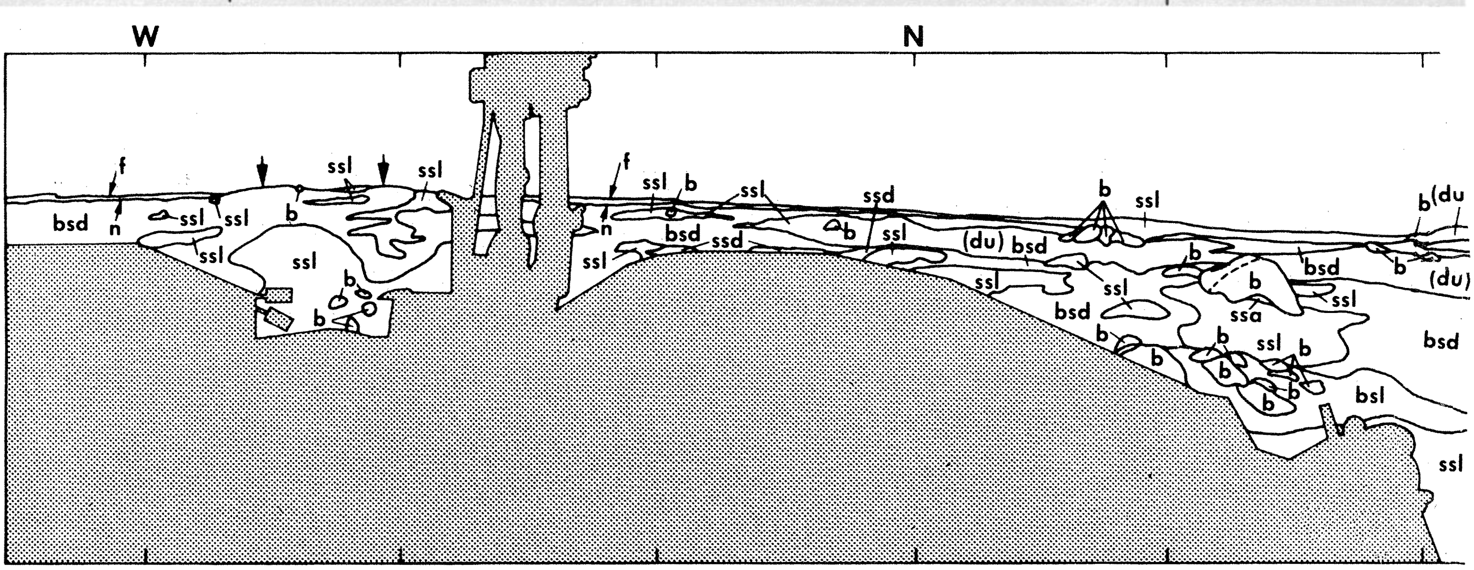

Fig. 5 (top). The second panorama was taken on sol 3 with camera 1. The central region reveals the landscape not previously imaged in Fig. 2. The large boulder northeast of the lander is about 8 m away and about 3 m high. Behind the surface sampler arm is a small dune field. Refer to Fig. 6 for sketch map of this landscape. This panorama, combined with Fig. 2, provides stereo coverage of about 240° in azimuth. Fig. 6 (bottom). Viking lander 1, sol 3, camera 1 survey panorama terrain sketch map, compiled from enlargements of returned Viking 1 lander images. The sketch map covers an azimuth range of about 300°. Several terrain units were mapped. The scene is dominated by light and dark blocky surface material (*bsl* and *bsd*) with block sizes ranging from centimeters in the near field to tens of meters near the horizon. The blocks are frequently angular and show no obvious preferential orientation. Block surface density is relatively uniform on the scale of tens of meters, although the nal calibration lamps—at least for the photodiode channels used in the measurements discussed in this report. More reliable data reduction must also include the use of at least one of three reference test charts on the lander (see Fig. 4). These charts consist of calibrated color and gray reflectance patches. However, their use for absolute radiometric camera calibration is made difficult because the exact amount of light falling onto the reference test chart is difficult to assess. Total lighting includes contributions from direct sunlight as well as skylight, some of which may be reflected off the lander structure onto the charts.

As illustrated in Figs. 1 and 5 and on the cover, the brightness of the martian sky is comparable to that of the surface. This skylight is produced by air molecules and suspended particles, which scatter the sunlight incident on the atmosphere from above and reflected by the surface from below. Preliminary quantitative studies of imagery from the first week of Viking 1 lander operations, as discussed below, provide estimates of the relative contributions from particles and molecules, the abundance of suspended particles, their composition, time variation, and mean size.

The relative importance of the contributions of air molecules and particles to the observed skylight can be assessed by examining its observed absolute brightness. We express this brightness in terms of r, the ratio of the observed brightness to that expected from a perfectly reflecting Lambert scattering surface at Mars' distance from the sun which is illuminated by sunlight falling normal to its surface. For the sol 0 panorama, $r \simeq 0.2$ at

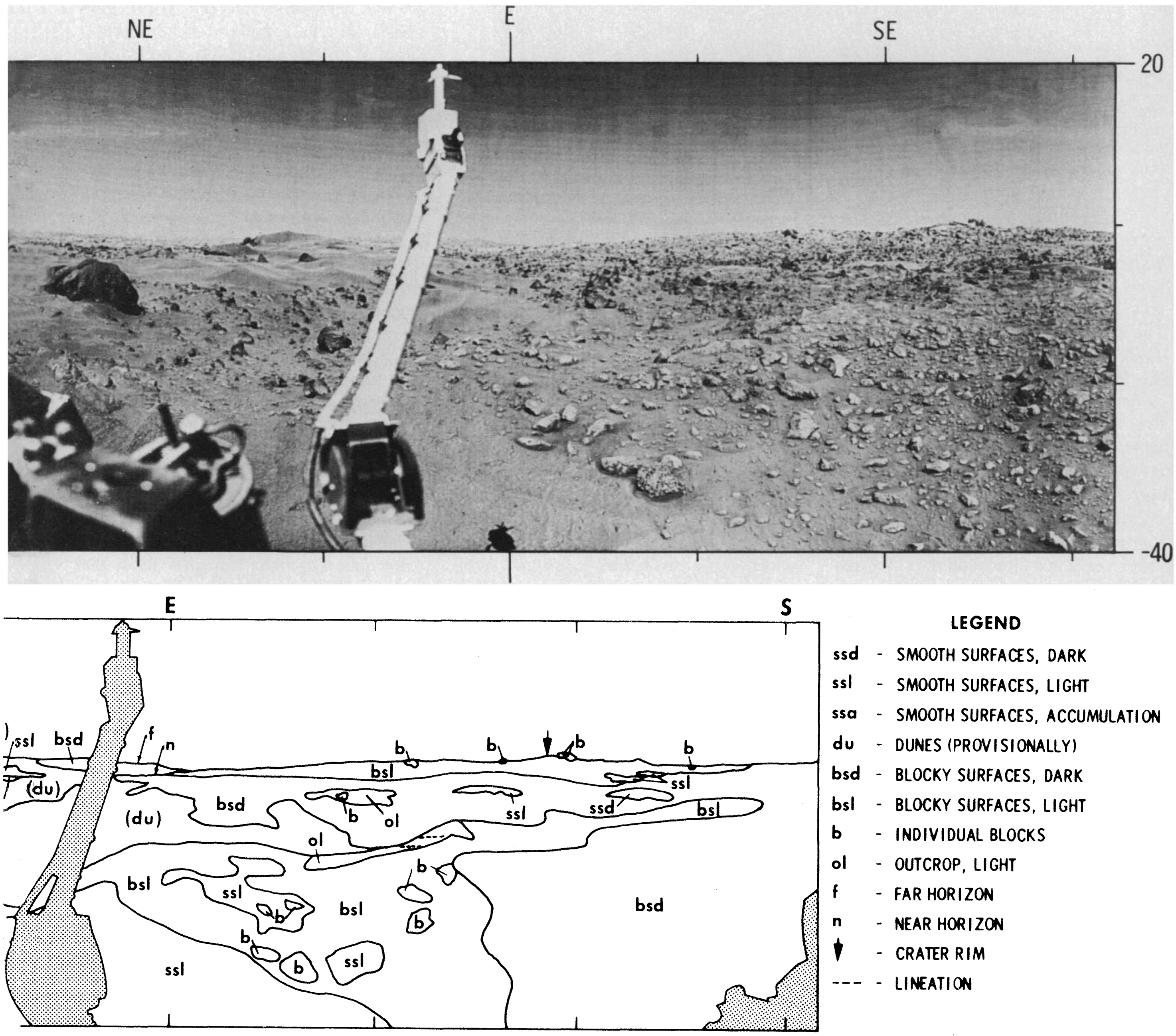

distribution is patchy at smaller scales. In the *bsl* and *bsd* units, there are interblock areas of fine-grained loosely consolidated material with variable albedo: light (*ssl*) and dark (*ssd*) surface materials are mapped. An *ssa* unit is used to denote an accumulation of smooth material, probably emplaced by aeolian processes. The (*d*) material is assumed to be a dune field. Three small lineaments have also been mapped, including two lineaments in one of the light outcrop (*ol*) units and what appears to be a fracture or ledge in the largest block in the scene. Possible crater rims on the horizon are delineated by vertical arrows where considered fairly definite. Blocks are outlined where prominent due to size or where intersecting a terrain contact. The near horizon is denoted by *n* and the far horizon is denoted by *f*. The nominal horizon is calculated to be about 3 km distant. Compass headings are indicated across the top of the scene.

Fig. 7. This blocky surface extends from a few meters from the lander out to the highest point on the local horizon (150 ± 75 m). There are several smooth mounds in the background that appear to be dunes of windblown sediment. At the right in the middle of the frame is a patch of fractured and jointed rock that may be an outcropping.

an elevation angle of 15° and an angular distance β of 90° from the sun. Somewhat smaller values pertain at larger β and somewhat larger values at smaller β. The effective wavelength of the survey diode used for this picture, weighted by the transmittance characteristics of the camera and the solar spectrum, is $\simeq 0.73$ μm. For an optically thin Rayleigh scattering atmosphere, the measured surface pressure of the landing site, and the above geometry, we find (16) that the value of r expected solely from molecular scattering is ~ 0.0003 times the observed value of r. Thus almost all the sky brightness is due to scattering by particles present in the atmosphere.

For an elevation angle of 10° and a scattering angle of 50° on the sol 0 panorama, $r \simeq 0.3$. To estimate the extinction optical depth τ we assume that $\tau < 1$ and thus that the observed skylight is principally due to singly scattered sunlight. We find (16) that $\tilde{\omega}_0 p \tau \simeq 0.2$, where $\tilde{\omega}_0$ and p are, respectively, the single scattering albedo and the scattering phase function at 50°. For many different phase functions $p \simeq 1$ at 50°. Also, at a wavelength of 0.73 μm, $\tilde{\omega}_0 \simeq 1$ because of the high brightness of Mars in the red. Thus $\tau \simeq 0.2$, and the amount of suspended particles in the martian atmosphere over the Viking 1 lander is comparable to values typical of continental areas on the earth. This value for τ is intended merely as an order of magnitude estimate.

The cover picture indicates that the sky is an orange cream to pink. We employ the color composite obtained on sol 1 to obtain $C \equiv r(\text{red})/r(\text{blue})$, where r(red) and r(blue) are, respectively, r values for the sky in the red and blue pictures. A value $C = 1$ implies a gray sky, while $C > 1$ means preferential scattering of red light. Note that C is independent of the spectrum of the incident sunlight, while the color pictures shown on the cover exhibit the product of C and the solar spectrum. From observed values of r and ground-based calibration of the camera, we find that $C \simeq 2.5$. However, comparison of r for the test charts with values predicted from the ground-based calibration indicates that the latter give values of C that are about 25 percent too large. With this correction we find that $C \simeq 1.9$. Part of the discrepancy could be caused by a contribution to the light incident on the test chart from a red-colored sky. In any event, $1.9 < C < 2.5$.

These values of C provide information on particle composition. The two leading candidates are soil particles blown into the atmosphere by strong winds and water ice particles formed by atmospheric condensation. Very small ice particles—that is, ones much smaller than the wavelength of visible light—will have a much larger cross section for scattering blue than red light, and thus $C \ll 1$. Larger ice particles will have extinction cross sections more nearly comparable in the two colors. Because ice is very transparent at visible wavelengths, the extinction cross section will be identical with the scattering cross section. Hence, at most angles of scatter, $C \simeq 1$ for ice. Allowance for light reflected from the surface and subsequently reflected again by the atmospheric particles slightly increases C to about 1.1. Thus the observed value of C is inconsistent with values expected from ice particles. However C significantly > 1 is consistent with the presence of red surface particles suspended in the atmosphere. Surface particles large enough to have comparable extinction cross sections in blue and red light would preferentially absorb blue light while preferentially scattering red light. A conservative *lower* bound on the mean particle radius needed to meet this condition is 0.1 μm. Several lines of evidence suggest that the particles suspended in the great 1971 martian dust storm were ~ 1 μm in radius (13).

The sky brightness values obtained on different days for similar lighting geometries are very similar, suggesting that we are not witnessing a transitory or isolated dust storm passing over the landing site (none was detected by Viking orbital photography), but rather a background aerosol that is present over large areas of

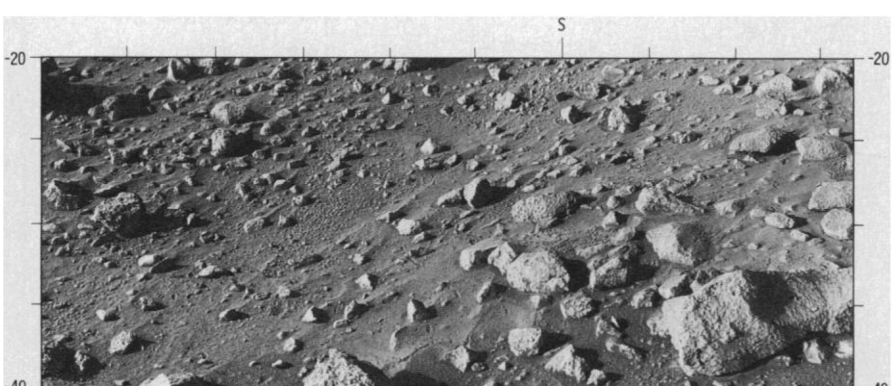

Fig. 8. This picture illustrates the variety of rock textures from smooth to extremely pitted or vesicular. Near the center is a pebbly patch that is probably analogous to a terrestrial lag gravel. Most of the rocks in this scene have depressions on the presumed windward side and elongated piles of sediment to the lee. There are numerous small pits, particularly in the lower center, that probably formed during landing, as material thrown out by the retrorocket exhaust impacted near the lander.

the planet for much of a martian year. The martian season of our observations is antipodal to the times when global dust storms arise. The optical depth of this background aerosol may vary on time scales of months, but the important point is that τ may be appreciable much of the time.

The presence of large quantities of partially absorbing dust particles in the atmosphere implies that the dust particles are an important source of atmospheric heating. As a result, the lapse rate in the upper portion of the troposphere may be more subadiabatic and the height of the convection zone during the day may be shallower than values pertinent to dust-free conditions. Also, a considerable depth of the lower atmosphere may undergo significant diurnal temperature fluctuations, which may in turn generate diurnal variations in atmospheric pressure and winds; in contrast, when there is no suspended dust the atmosphere is warmed chiefly from the surface, and only a shallow lower region of the atmosphere would experience significant diurnal temperature fluctuations. It is interesting to note that rather large diurnal fluctuations in surface pressure and winds have been detected by the Viking lander meteorology experiment (*17*).

Surface photometric properties. The presence of a bright sky may imply that skylight has made an important contribution to light from Mars observed by past flyby and orbiter missions, and by ground-based observations, and could have biased previous estimates of the surface albedo. This is substantiated by very preliminary analysis of Viking orbiter and lander image data. While analysis of Viking orbiter imagery (*4*) suggests that the mean albedo in the landing ellipse is higher than the mean albedo of Mars averaged over bright and dark areas, analysis of initial Viking lander imagery suggests that the local albedo is lower than this average value. Alternatively, the Viking lander may have touched down in an area which has a lower albedo than the regional average, such as near a dark-haloed crater or on a dark streak.

Lander imagery data—both the sol 0 survey and the sol 1 color picture—were reduced as follows. Images were divided into small (20° by 20°) sections covering the unobstructed portion of the martian surface between the meteorology boom and the RTG windscreen. The brightness in each section was then calculated for a flat surface using three theoretical photometric functions: a near-Lambertian surface, an empirical function (*15*) based on

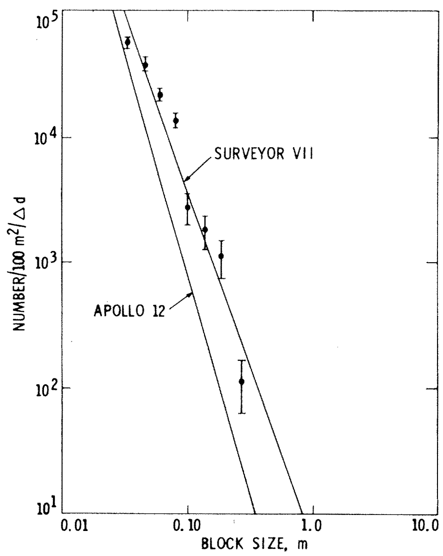

Fig. 9. Block size distributions for Viking lander 1 site, taken from the sol 0 survey image (Fig. 2). Counts are plotted as incremental frequencies per area. Error bars are binomial sampling standard errors about most probable values. Apollo 12 and Surveyor 7 plots are shown for comparison.

Mariner 9 data, and a lunar-type backscattering surface. These predictions (*3*) were then compared with measured values of surface brightness averaged over the same image sections. The best agreement was found for an albedo lower than the average Earth-based value for Mars and for a lunarlike backscattering surface. This result implies that, on the scale of at least a few micrometers, the surface may have a complex microrelief, porosity, and fine-grain size distribution not very dissimilar from those of lunar regolith. Preliminary quantitative reduction of the sol 1 three-color images indicates a surface reflectivity spectrum in the visual wavelength range which is consistent with Earth-based observations.

Motion detection and variable features. The imaging investigation includes a search for variations in the scene caused by windblown dust, albedo changes in the surface material, or, possibly, motion of macroscopic organisms (macrobes).

In the variable features experiment, a half-dozen regions on the surface and a grid target atop the lander are monitored at 1- to 10-day intervals at similar sun elevations. Preliminary studies have shown no changes on the surface besides those produced by ejection of the sampler arm shroud and locking pin. The shroud eject exposed a surface darker than the overlying material, and the area is being examined for albedo change due to dust deposition and chemical weathering. The grid target appears to be particle-free and it therefore seems that material was not raised to the level of the lander body (~ 1 m) after landing.

The motion of objects that are larger than several picture elements appears primarily as geometric distortion, rather than blurring of detail as in film cameras. It is difficult to classify the extent of geometric distortion in a general sense, as, for example, by recognition limits as a function of object size and velocity, because the extent of geometric distortion depends not only on these factors but also on the direction of object motion (*18*). No obvious examples of this type of distortion have been observed. An example of unusual features parallel to the scan direction is seen in the leftmost portion of the sol 0 picture (Fig. 1) of the footpad (*5*).

There is a repeated scanning mode in which the camera azimuth advance is inhibited and a scene which is one resolution element in angular width is repeatedly imaged with a period of either 0.22 or 14.13 seconds (Fig. 10). During the first week of imaging this mode was exercised for a total of about 35 minutes (primarily at the longer period) during both middle morning and late afternoon. The only variations observed thus far can be explained by brightness changes caused by sun movement during the imaging, and elongation of shadows projected by large rocks or the lander itself.

The dearth of observable changes to date is consistent with the low seasonal winds as measured by the meteorology instrument. The theoretical wind velocity in the boundary layer required to induce particle saltation (*13*) is several times greater than the highest gust velocities recorded (*16*). However, the repeated scan technique is extremely sensitive to changes as subtle as the vibration of a single specularly reflecting particle well below the resolution of the camera optics, and it is possible that meteorology results combined with such observations will yield the threshold velocity for particle movement, during anticipated periods of higher winds later in the mission.

Biology. With the discovery by the Viking entry mass spectrometer (*19*) and by the lander gas chromatograph–mass spectrometer (*20*) of molecular nitrogen in the martian atmosphere, all essential prerequisites for a martian biology based on terrestrial biochemistry have been satisfied: CO_2, H_2O, N_2, and sunlight. But necessary conditions are, of course, not the same as sufficient ones, and the question must be settled experimentally. The Viking 1 lander camera has a resolution

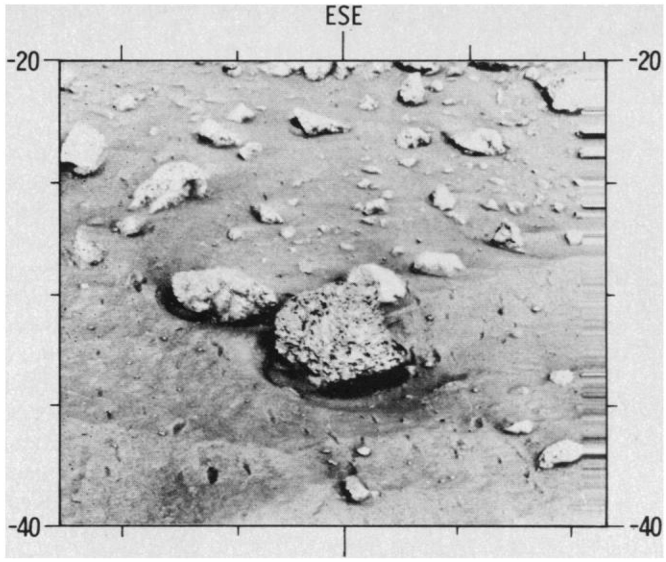

Fig. 10. The semicircular depressions around the two rocks at the center of this picture are clear evidence of wind scouring. Indirectly they also demonstrate that much of the surficial material is in the size range that can be eroded and transported by high winds, probably between 50 and 300 μm. The larger rock has a very rough texture and appears to be crudely banded. Numerous small depressions in the surface around the rocks probably formed at landing. The darker interiors of the pits suggest that subsurface fine material is darker than surficial material. The array of parallel bright and dark lines along the right-hand edge of this picture is a representation of the repeated single-line scan capability of the Viking cameras. The absence of left-right variability in this rescan mode indicates no motion at this time and place.

ranging from a few millimeters in the near field to 2 m at the nominal horizon 3 km away, when run in the high-resolution (0.04°) mode. Similar panoramic photographs obtained in most places on the land area of Earth would show unambiguous signs of life—largely grasses, bushes, and trees. No apparent signs of life would be obtained by such photographs taken on the surface of the terrestrial oceans, which comprise some 60 percent of the surface area of the earth, or in some desert and polar regions, comprising at least a few percent of the land area of the earth. While the Viking biology experiments tend principally toward microbiology, it has been thought possible that large organisms also exist on the planet (*21*), and one of the objectives of the imaging experiment has always been (*1*) the search for such macrobes.

In the 2×10^{-7} percent of the surface area of Mars accessible in varying resolutions to the Viking 1 lander camera, and in the first week of imagery, no apparent signs of life have been detected—for example, arrays of complex morphological forms exhibiting elaborate bilateral symmetry, or top-heavy forms in strong mechanical disequilibrium. In the polychromatic imagery there are no patches of anomalous color to suggest photosynthetic pigments. Comparison of both repeated single line scans and full pictures reveals no relevant changes in the configuration of surface features. There are no pits, hollows, or furrows which are uniquely attributable to mobile organisms, nor were any other features discerned which might plausibly be considered spoor. There are no objects which are obvious artifacts of intelligent life. Possible models of martian biology exist in which organisms are, because of the high ultraviolet flux, largely subsurface or largely coated with rocklike ultraviolet shields; or in which the photosynthetic pigments are red or black; or in which, in order to obtain access to brief periods of available liquid water, organisms live in shadows; or in which the macrobes do not reside in this time or place. The search for martian macrobes or their fossil equivalents by the Viking spacecraft will continue.

Lander orientation and geometry. The position of the sun in the martian sky at a specified place and time on Mars is known from astronomical observations of the relative location of Mars and the sun. We therefore know something about the expected shadows cast by the lander onto the martian surface at the time and place of landing, and how these shadows are likely to appear in the first few pictures sent back by the lander cameras. Since the lander is a very irregular object, its shadow profile changes radically depending on how the lander is oriented relative to the sun. From this information we are able to ascertain to within about 1° of accuracy the azimuth of the lander relative to the sun by comparing the shadow profile observed in the sol 0 panorama with the shadows cast by a 1/6 scale model of the lander. By more careful comparison of shadows, we can obtain an estimate of the lander tilt to an accuracy of about 5°. We achieve this comparison both by illuminating the model with a collimated light source to simulate the shadow profile produced by the sun, and by mathematically connecting particular shadow points with the positions of objects on the lander which cast them. Our result for lander orientation is 321.4° ± 1° east of north for leg 1, and < 5° for lander tilt.

We have also fit a plane to a series of lines from the camera to points on the horizon for the survey picture, using the method of least squares. From this we determine the relationship between the lander horizontal plane and the plane that contains the seven vectors and the coordinate system origin. We find an azimuth of 321° and a slope of 3.6°.

For comparison, planned orientations were, respectively, about 324° and 0°. The accelerometer readout gave, respectively, 321.91° and 2.99°. The azimuth direction of downward tilt is 285.17° clockwise from north. Thus, all data are consistent with an orientation azimuth of 321° to 322°, and a slope of the lander away from horizontal of 3° to 4°. These values were employed in a computer transformation of the apparent horizon sinusoid (Figs. 2 and 5) to a horizontal line (local relief excepted).

THOMAS A. MUTCH
Department of Geological Sciences, Brown University, Providence, Rhode Island 02912
ALAN B. BINDER
Institut für Geophysik, University of Kiel, Federal Republic of Germany, and Science Applications, Inc., Pasadena, California 91101
FRIEDRICH O. HUCK
Flight Instrumentation Division, NASA Langley Research Center, Hampton, Virginia 23665
ELLIOTT C. LEVINTHAL
Department of Genetics, School of Medicine, Stanford University, Stanford, California 94305
SIDNEY LIEBES, JR.
Department of Genetics, School of Medicine, Stanford University
ELLIOT C. MORRIS
Branch of Astrogeologic Studies, U.S. Geological Survey, Flagstaff, Arizona 86001
WILLIAM R. PATTERSON
Division of Engineering, Brown University
JAMES B. POLLACK
Space Science Division, Ames Research Center, Moffett Field, California 94305
CARL SAGAN
Laboratory for Planetary Studies, Cornell University, Ithaca, New York
GLENN R. TAYLOR
Viking Project Office, NASA Langley Research Center

References and Notes

1. T. A. Mutch, A. B. Binder, F. O. Huck, E. C. Levinthal, E. C. Morris, C. Sagan, A. T. Young, *Icarus* **16**, 92 (1972).
2. F. O. Huck, H. F. McCall, W. R. Patterson, G. R. Taylor, *Space Sci. Instrum.* **1**, 189 (1975).
3. F. O. Huck and S. D. Wall, *Appl. Opt.* **15**, 1748 (1976).
4. M. Carr *et al.*, *Science* **193**, 766 (1976).
5. The left side of the footpad picture contains two particularly interesting features. Neither is a real surface feature, since they do not appear in later images of the same area. The first picture was taken about 25 seconds after touchdown. In the first 75 lines of the picture, which took 15 seconds to acquire, there are a large number of fine, bright striations in the image. The effect is similar to what one would expect if the scene illumination were varying markedly from line to line; that is, on a time scale of 0.2 second. The cameras show no electrical anomalies and there were no activities scheduled on the lander which might have caused electrical interference. These lines might be the result of a turbulent cloud of fine dust raised by the lander's retrorockets. Since the lines are brighter than the scene, the dust must, in this explanation, be between the camera and the surface region viewed. The scene detail is not degraded. The turbulence would have to vary very rapidly, and, to the extent that the effect influences entire scan lines, the turbulence would have been correlated over distances of 75 cm. Dust seems to be a plausible explanation, although we have not yet completed our analysis of the time and space variations of these early digital data. The second feature is a distinct vertical dark band crossing the picture. Several explanations might be proposed. First, the dark band could be the shadow of the lander's parachute passing the lander. However, the duration of the shadow is inconsistent with the diameter of the parachute and the wind velocity. Second, it is possible that the band could be the shadow of a martian cloud, in which case other similar bands should be seen as the mission progresses. Through sol 7 no other such bands have been detected. Third, the band could be produced by clods of regolith ejected during descent maneuvers, rapidly deposited on the camera window and slowly sliding off. However the time delay between landing and the appearance of the dark band seems to rule out this explanation. Finally, the dark band could be the shadow of a cloud of dust raised by the landing. This model has been investigated and is consistent with the parameters of the landing if the cloud is roughly 100 m across and 200 m above the surface. Applying the Stokes-Cunningham equation to the particles in the cloud yields an upper limit on particle diameter of roughly 200 μm, a plausible value.
6. E. C. Morris, T. A. Mutch, H. E. Holt, *Atlas of Geologic Features in the Dry Valleys of South Victoria Land, Antarctica; Possible Analogs of Martian Surface Features* (U.S. Geological Survey Interagency Rept.; Astrogeology 52, 1972).
7. E. Morris and E. Shoemaker, *Icarus* **12**, 188 (1970).
8. R. Arvidson, R. Drozd, E. Guinness, C. Hohenberg, C. Morgan, *Proceedings of the 7th Lunar Science Symposium*, in press.
9. H. Moore, R. Pike, G. Ulrich, "Lunar terrain and traverse data: Lunar roving vehicle design study" (U.S. Geological Survey, informal report, 1969).
10. C. Sagan *et al.*, *J. Geophys. Res.* **78**, 4163 (1973); *Icarus* **17**, 346 (1972); J. Veverka *et al.*, *ibid.* **21**, 317 (1974).
11. The Viking cameras record picture information on one or more of 12 silicon photodiodes positioned in the focal plane. The photodiodes are sensitive to light from approximately 0.4 to 1.1 μm in wavelength. Six of the diodes are covered with interference filters which transmit light only in selected wavelength ranges. In acquiring a color picture, data are recorded with three photodiodes which have blue, green, and red filters. Three filtered photodiodes in the near infrared are used to acquire infrared imagery. Color data returned to the earth are used in the laboratory to modulate the intensities of red, green, and blue light ray bundles which are simultaneously scanned over a sheet of color film. Because the voltages recorded by the diodes are a complex function of the diode sensitivities, the filter characteristics, and the atmospheric transmission, it is necessary to scale the relative contributions of each of the three channels to compensate for these effects. The necessary compensation has been calculated in two substantially independent ways which yield similar results. One method depends on prelaunch measurements of the relative spectral responsivities and of the absolute response to a broadband light source to compute the compensation required for equal output for a neutral gray reflecting scene. This assumes that the cameras are stable and that the atmospheric attenuation is negligible. The second method depends on the measured camera response to viewing a reference target (Fig. 4) on the lander top. This target has red, green, and blue color reference patches and also 11 gray patches with integrated reflectances between 0.1 and 0.9. The color compensation is adjusted to optimize the target reproduction; then that compensation is applied to the scene. The disadvantage of this technique is the uncertainty in the human judgment of the "best" reproduction of the target. Both techniques are complicated by the fact that some of the interference filters have small "leaks." For example, the blue filter transmits a small amount of light in the infrared. An object in the scene which reflects large amounts of light in the infrared will appear deceptively bright when imaged with the blue diode. In order to determine such spurious contributions from the scene it is necessary to obtain both a color and an infrared picture of the same scene under approximately the same illumination conditions, and then to balance the colors in a manner which is empirically consistent with the data. Among other reasons for accepting the reality of the colors portrayed, however, is the correct rendering of the gray spacecraft surface and the orange cables.
12. A. Dollfus, *Ann. Astrophys. Suppl. 4* (1957) (NASA Tech. Transl. TT-F-188); A. Binder and D. Cruikshank, *Commun. Lunar Plan. Lab. 193* (1964); R. A. van Tassel and J. W. Salisbury, *Icarus* **3**, 264 (1964); C. Sagan, J. P. Phaneuf, M. Ihnat, *ibid.* **4**, 43 (1965); J. B. Pollack and C. Sagan, *Space Sci. Rev.* **9**, 243 (1969).
13. O. B. Toon, J. B. Pollack, C. Sagan, *Cornell Univ. Rep. CRSR 639* (1976); *Icarus*, in press.
14. R. L. Huguenin, *Icarus* **28**, 203 (1976).
15. T. Thorpe, *ibid.* **20**, 482 (1973); personal communication.
16. J. Pollack, *Icarus* **6**, 42 (1976).
17. S. Hess *et al.*, *Science* **193**, 788 (1976).
18. F. O. Huck, S. D. Wall, E. E. Bucher, *NASA TND-7668* (1974).
19. A. Nier *et al.*, *Science* **193**, 786 (1976).

T. Owen and K. Biemann, *ibid.*, p. 801.

21. C. Sagan and J. Lederberg, *Icarus* **28**, 291 (1976).
22. A large number of people have made substantial contributions to this report, in areas of mission design and science analysis. In a very real sense, these persons should be considered coauthors. They include R. E. Arvidson, P. Avrin, C. E. Carlston, R. D. Collie, N. Coradini, R. E. D'Alli, E. W. Dunham, P. L. Fox, S. U. Grenander, E. A. Guinness, B. W. Hapke, J. W. Head, K. L. Jones, R. A. Kahn, B. K. Lucchitta, D. Nummedal, D. C. Pieri, C. W. Rowland, R. S. Saunders, R. H. Stockman, R. B. Tucker, S. D. Wall, and M. R. Wolf. Andrew T. Young played an important role in the early design studies of the lander imaging system. A number of college undergraduates assisted in the operational phase of the investigation. They include A. L. Chaikin, R. G. Cooper, W. E. Dieterle, C. Eberspacher, F. D. Eckelmann, Jr., E. A. Hildum, H. W. Printz, D. W. Thompson, and J. C. Thompson. Their participation was made possible by support from the Alfred P. Sloan Foundation and by the NASA Planetology Office. Because the success of each science investigation is crucially dependent on the efforts of the 750 members of the flight team headed by J. S. Martin, Jr., Viking project manager, and A. Thomas Young, Viking mission director, as well as the 10,000 contractor employees who designed and built the spacecraft, its components, and support equipment, our acknowledgement should also include the 10,000 signatures in the microdot carried to Mars on the spacecraft (Fig. 4). Design and manufacture of the Viking lander cameras was performed by the ITEK Corporation, with active cooperation by Langley Research Center and Martin Marietta Corporation. The Image Processing Laboratory, Jet Propulsion Laboratory, is responsible for special processing of imaging data returned from Mars to the earth and processed the images in Figs. 2, 5, 7, 8, and 10. The images in Figs. 1 and 4 were processed with the real-time software developed by the Data Systems Division of JPL. Financial support for the work of team members was provided by the NASA Viking Project Office.

30 July 1976

Composition of the Atmosphere at the Surface of Mars: Detection of Argon-36 and Preliminary Analysis

Abstract. *The composition of the martian atmosphere was determined by the mass spectrometer in the molecular analysis experiment. The presence of argon and nitrogen was confirmed and a value of 1 to 2750 ± 500 for the ratio of argon-36 to argon-40 was established. A preliminary interpretation of these results suggests that Mars had a slightly more massive atmosphere in the past, but that much less total outgassing has occurred on Mars than on Earth.*

The objective of the Viking molecular analysis experiment is twofold: to detect and identify the organic compounds, if any, present in the surface of Mars, and to determine periodically the composition of the lower atmosphere (*1*). The central part of the instrumentation for this experiment is a mass spectrometer, coupled to a gas chromatograph for the organic analysis and, by way of a molecular leak, to a gas sample reservoir. Although the instrument was designed primarily for the detection of organic compounds in the gas chromatographic mode (*2*), the mass spectrometer's high sensitivity (dynamic range, six to seven orders of magnitude), high mass range (m/e 12 to 200), and resolution (1 : 200 at m/e 200; better at lower mass) were used to advantage in determining the composition of the atmosphere, particularly its minor constituents. The penalty one pays for resolution and sensitivity is a certain loss of accuracy, mainly because the residual background in the instrument becomes more significant and the long-term reproducibility of the fragmentation pattern is lowered.

Since the more important questions concerning the composition of the martian atmosphere centered around the minor components and certain isotopic ratios, an attempt was made to optimize the experiment toward that goal. In particular, the detection of even traces of N_2 was deemed to be extremely important because previous data (*3*) suggested that it must be a minor component or could be almost completely absent (*4*). One of the major problems in a mass spectromet-